SCIENTIFIC REPORTS

OPEN

Bulk RKKY signatures of topological phase transition in silicene

Received: 4 October 2017
Accepted: 27 March 2018
Published online: 18 April 2018

Hou-Jian Duan[1], Chen Wang[2], Shi-Han Zheng[1], Rui-Qiang Wang[1], Da-Ru Pan[1] & Mou Yang[1]

Silicene offers an ideal platform for exploring the phase transition due to strong spin-orbit interaction and its unique structure with strong tunability. With applied electric field and circularly polarized light, silicone is predicted to exhibit rich phases. We propose that these intricate phase transitions can be detected by measuring the bulk Ruderman-Kittel-Kasuya-Yosida (RKKY) interaction. We have in detail analyzed the dependence of RKKY interaction on phase parameters for different impurity configurations along zigzag direction. Importantly, we present an interesting comparison between different terms of RKKY interaction with phase diagram. It is found that the in-plane and out-of-plane terms can exhibit the local extreme value or change of sign at the phase critical point and remarkable difference in magnitude for different phase regions. Consequently, the magnetic measurement provides unambiguous signatures to identify various types of phase transition simultaneously, which can be carried out with present technique.

Topological quantum phase transition has received great interest in condensed matter of states for searching for new matter states[1], such as very recently emerging topological insulators (TIs), Weyl or Dirac semimetals. Topological quantum state possesses many exotic and robust properties with potential application in quantum calculations[2,3]. Topological phases are usually classified with topological indices. In 2D quantum system, the topological indices are reduced to the charge- and spin-Chern numbers[2], obtained by summation over the Berry curvature. Nevertheless, how to identify these different topological states experimentally is a challenging problem. The most instinctive method to detect a topological phase is to measure the spin-resolved quantum Hall conductivity or to directly probe topological states. However, these electric measurements are difficult to perform in quantum Hall systems and moreover topological edge states are easy to suffer from the disturbance from bulk states which are unavoidable due to the existence of imperfections in the composition.

Much effort is made to find other new tools for probing the topological phase transition. The phase-dependent heat currents provide a robust tool to distinguish the existence of topological Andreev bound states from trivial Andreev bound states in superconductor/TI Josephson junction[4]. To explore the existence of fractional quantum Hall states in TIs, authors[5] presented thermoelectric measurements on the Bi_2Te_3 crystal. The magnetic susceptibility of electrons was studied in topological nodal semimetals, in which a giant anomaly is regarded to be useful in experimental identification of the Weyl, Dirac and line node semimetals[6]. The spin response in HgTe quantum wells[7] reveals that unconventional spin-related properties can distinguish the paradigmatic TI material from the other 2D electronic systems.

Silicene, a single layer of silicon atoms with a planar honeycomb lattice structure[8–10], offers an ideal platform for exploring the phase transition. Besides large spin-orbit interaction up to 3.9 meV[11], silicene possesses a buckled hexagonal structure, in which two atoms in the translational unit cell reside on different planes, making its bandgap tunable easily by applying an electric field perpendicular to the silicene sheet[12]. The electric field breaks inversion symmetry while the circularly polarized light breaks time-reversal symmetry, both of which modify the Berry curvatures in the momentum space so that the occupied electronic states change the topological properties. When both of fields are applied, the silicene is predicted to exhibit rich phases: quantum spin Hall insulator (QSHI), conventional bulk insulator (CBI), photoinduced quantum Hall insulator (P-QHI), and photoinduced spin-polarized quantum Hall insulator (PS-QHI)[13]. It is an intriguing problem how to detect experimentally

[1]Guangdong Provincial Key Laboratory of Quantum Engineering and Quantum Materials, School of Physics and Telecommunication Engineering, South China Normal University, Guangzhou, 510006, China. [2]School of Information Engineering, Guangdong University of Technology, Guangzhou, 510006, China. Correspondence and requests for materials should be addressed to R.-Q.W. (email: rqwanggz@163.com) or D.-R.P. (email: pandaru@126.com)

which phase the system stays in just by the bulk property. To probe these intricate phase transitions, Jin *et al.*[14] have suggested to measure the Nernst conductivity, from which phase boundaries can be determined by comparison the charge- with spin-Nernst conductivities.

The Ruderman-Kittel-Kasuya-Yosida (RKKY) interaction, which describes the indirect exchange coupling between magnetic impurities mediated by the itinerant electrons, greatly depends on the spin-orbit interaction of host materials[15]. Meanwhile, the spin-orbit interaction plays a vital role in topological phase transitions. Thus, it is natural to expect that there is a close relation between the RKKY interaction and phase transition. For the phase transition from QSHI to CBI induced by electric field, Zare *et al.*[16] found that the RKKY interaction can be used to identify the topological phase since its RKKY interaction is about 20 times greater than in the band insulator region when impurities are located on the edge. However, no difference in the order of magnitude appears in the case where the magnetic impurities are in the bulk. In this paper, we extend this study to more intricate phase transitions when silicene is subjected to both a circularly polarized light and a perpendicular electric field, where four types of phase are involved: QSHI, CBI, P-QHI, and PS-QHI. We have in detail analyzed dependence on phase parameters of RKKY interaction and present a RKKY phase diagram. It is interesting to find that the RKKY measurement provides unambiguous signatures to identify different phases and phase boundaries simultaneously. Moreover, all signatures originate from the bulk band and thus one can probe the topological phases only by measuring the bulk states, not caring for the formation of topological states.

Model and Method

Silicene has a honeycomb lattice with two different atoms in the translational unit cell. Employing the tight-binding model for the four bands[13], the Hamiltonian is given by[16]

$$H=-t\sum_{\langle i,j\rangle s}c_{is}^{+}c_{js}+i\frac{\lambda_{so}}{3\sqrt{3}}\sum_{\langle\langle i,j\rangle\rangle ss'}c_{is}^{+}\sigma_{ss'}\cdot(\mathbf{d}_i\times\mathbf{d}_j)c_{js'}+U\sum_{is}\mu_i c_{is}^{+}c_{is}\tag{1}$$

where $\langle i,j\rangle$ ($\langle\langle i,j\rangle\rangle$) runs over the nearest-neighbor (next-nearest-neighbor) hopping sites, c_{is}^{+} creates an electron with spin s at site i, σ is the Pauli matrix of spin, $\mathbf{d}_i$ and $\mathbf{d}_j$ are the in-plane unit vectors along which the electron traverses from site j to i. The first two terms describe the silicene with hopping energy $t=1.6\,\text{eV}$ and the intrinsic spin-orbit coupling $\lambda_{so}\approx 3.9\,\text{meV}$[11,17,18], while the weak Rashba spin-orbital interaction is neglected[13]. The third term stands for the staggered potential with $\mu_i=\pm 1$ for A (B) site and $U=E_z d/2$, caused by an electric filed E_z exerting on the buckled lattice structure[19–21], where two sublattice planes are separated by a distance of $d=0.46\mathring{A}$. By transforming Eq. (1) into the momentum space and then expanding it at the two Dirac points $\mathbf{K}_\eta$ ($\eta=\pm$) in the Brillouin zone (BZ), we in the pseudospin space $\{A, B\}$ obtain the low-energy Dirac Hamiltonian[16]

$$H_{\eta s}=\begin{pmatrix} U_{\eta s} & \hbar v_F k\Phi_{K_\eta}\\ \hbar v_F k\Phi_{K_\eta}^{*} & -U_{\eta s}\end{pmatrix}.\tag{2}$$

Here, $v_F=\frac{\sqrt{3}}{2}at$, $U_{\eta s}=-s\lambda_{so}\eta-U$ with $s,\eta=\pm 1$ are the spin and valley indices, respectively, and $\Phi_{K_\eta}=\eta e^{-i\pi/3+i\eta\theta}$ with the polar angle $\theta=\arctan(k_y/k_x)$ and an extra phase factor[22] stemming from the specific K_η.

In order to present rich phases, we assume the silicene sheet is in addition irradiated by a beam of circularly polarized light. The photoinduced effect is considered by the Peierls substitution $\hbar\mathbf{k}\to\hbar\mathbf{k}+e\mathbf{A}(t)$, where vector potential $\mathbf{A}(t)=A(\sin\omega t, \cos\omega t)$ is a periodic function of time $T=2\pi/\omega$ with ω being the light frequency. By using the Floquet theory[13,23–27], the time dependence can be mapped to a Hilbert space of time-independent multi-photon Hamiltonian. For the off-resonant light with the high-frequency limit $A^2/\omega\ll 1$, one can decouple the zero-photon state from the other states and only consider its dressed effect through second-order virtual photon absorption and emission processes[13,25,28,29]. As a consequence, the modified part of Hamiltonian by light reads $V_n=[V_{-1}, V_{+1}]/\hbar\omega+O(A^4)$ with $V_n=\frac{1}{T}\int_0^T H(t)e^{-in\hbar\omega t}dt$ and the effective Hamiltonian is approximately expressed as

$$H'_{\eta s}=H_{\eta s}+V_{n=0}=H_{\eta s}+\eta\Omega\sigma_z,\tag{3}$$

with the illumination parameter $\Omega=\frac{3t^2A^2}{4\hbar\omega}$. By diagonalizing the Hamiltonian $H'_{\eta s}$, the low-energy dispersion reads

$$E_{\eta s}^{\pm}=\pm\sqrt{\hbar^2 v_F^2 k^2+U_{\eta s}^2}\tag{4}$$

where the energy gap $2\left|U_{\eta s}\right|=2|(\Omega-s\lambda_{so})\eta-U|$ can be opened or closed, controlled by both the light and electric fields. Consequently, the topological phase transition occurs among four categories[13]: P-QHI, QSHI, PS-QHI, and CBI.

We assume two magnetic impurities $\mathbf{S}_i$ placed on the lattice sheet interacting with conducting electrons via $H_{int}=\lambda\sum_i\mathbf{S}(\mathbf{r}_i)\cdot\mathbf{s}(\mathbf{r}_i)$, where $\mathbf{S}(\mathbf{r}_i)$ [$\mathbf{s}(\mathbf{r}_i)$] is the spin of impurities (itinerant electrons) and λ is the spin-exchange coupling strength. For weak coupling, we can replace H_{int} with the RKKY interaction, which in the second-order perturbation theory[15,30–33] is given by

$$H_{RKKY}^{\alpha\beta}=\frac{-\lambda^2}{\pi}\text{Im}\int_{-\infty}^{E_F}\text{Tr}[(\mathbf{S}_1\cdot\sigma)G_{\alpha\beta}(\mathbf{R},\varepsilon)(\mathbf{S}_2\cdot\sigma)G_{\beta\alpha}(-\mathbf{R},\varepsilon)]d\varepsilon.\tag{5}$$

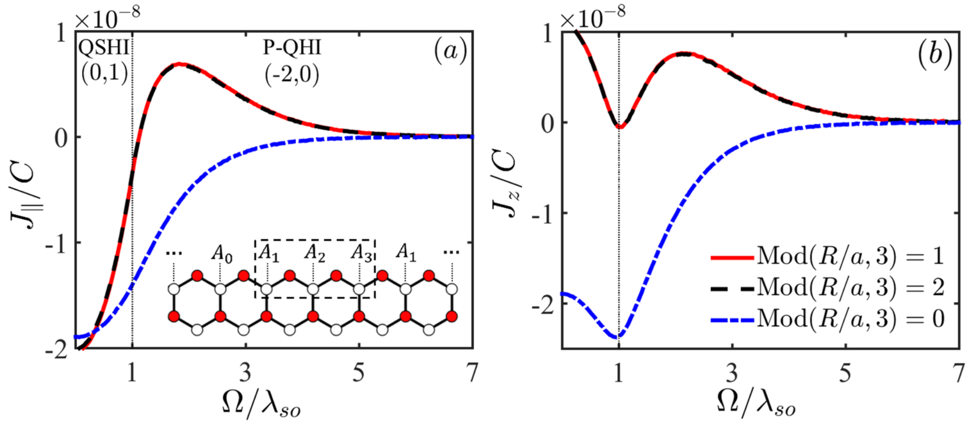

Figure 1. The variation of RKKY exchange coupling with illumination parameter Ω. The QSHI and P-QHI phases are divided by a vertical dotted line. Two impurities are distributed on the same lattice along the zigzag direction, as shown in inset, with three configurations in spatial distance $R=270a$ [Mod(R/a, 3) = 0], $271a$ [Mod(R/a, 3) = 1] and $272a$ [Mod(R/a, 3) = 2]. The other parameters are $E_F=0$, $t=1.6$ eV, and $\lambda_{so}=3.9$ meV.

Here, $\alpha, \beta=\{A, B\}$, $\mathbf{R}$ is spatial distance between two impurities, E_F is Fermi level, and the trace is over the spin degree of freedom. The retarded Green's function $G_{\alpha\beta}(\mathbf{R}, \varepsilon) = \sum_\eta \int e^{i(\mathbf{k}+\mathbf{K}_\eta)\mathbf{R}} d^2\mathbf{k} \left[1/(\varepsilon + i0^+ - H'_{\eta s})\right]_{\alpha\beta}$ is a 2×2 matrix in spin space. In next discussions, we focus on the impurities placed on the same sublattice (e.g., $\alpha=\beta=A$) and drop the subscript for briefness. Consequently, the matrix element of Green's function is diagonal in spin space and reads

$$G^s(\mathbf{R}, \varepsilon) = -\frac{2\pi}{\varsigma\hbar^2 v_F^2} \sum_{\eta=\pm 1} e^{i\mathbf{K}_\eta \mathbf{R}} (\varepsilon + U_{\eta s}) K_0(\mathcal{R}_{U_{\eta s}}), \tag{6}$$

where $K_0(x)$ is the modified Bessel function of the second kind, ς is the area of BZ, and $\mathcal{R}_x = R\sqrt{x^2 - \varepsilon^2}/\hbar v_F$ with $R=|\mathbf{R}|$. By inserting the above Green's functions in Eq. (5), the RKKY interaction can be rewritten as[16]

$$H_{RKKY} = J_\parallel \sum_{i=x,y} S_{1i}S_{2i} + J_z S_{1z}S_{2z} + J_{DM}(\mathbf{S}_1 \times \mathbf{S}_2)_z, \tag{7}$$

which is divided into three terms according to the polarizations of the impurities.

Numerical Results and Discussion

RKKY under light field. To detect the topological phases, we expect to search for signatures of the RKKY interaction characterizing the phase-transition point and various phase regions. Firstly, we consider the case of silicene sheet irradiated by a beam of off-resonant light but in the absence of electric field. The light field breaks the time-reversal symmetry and so causes spin splitting $|\Omega \pm \lambda_{so}|$ in the energy spectrum from the original spin-degenerate bands $s=\pm 1$. With the increase of light strength, the bandgap is closed first at the critical point $\Omega=\pm\lambda_{so}$ and then enters a new topological phase of P-QHI from QSHI state. Different topological phases can be classified by topological quantum numbers (C, C_s), corresponding to charge- and spin-Chern numbers, respectively. They are usually defined as $C = \sum_\eta (C_\uparrow^\eta + C_\downarrow^\eta)$ and $C_s = \sum_\eta (C_\uparrow^\eta - C_\downarrow^\eta)/2$, and are calculated with the integral of a closed path $C_s = \frac{1}{2\pi}\sum_n \int_{BZ} d\mathbf{k}\Omega_{xy}^n(\mathbf{k})$ over the Berry curvature $\Omega^n(\mathbf{k})$ of the n-th band[34]. Proceeding the calculation in silicene, we find that the topological index with different spins and valleys is $C_s^\eta = \frac{\eta}{2}\mathrm{sgn}(U - \eta\Omega + s\eta\lambda_{so})$. Thus, according to the relative value of external fields, we can differentiate phase regions with (C, C_s). For example, in the PS-QHI state, which is located in the area of $|\Omega - U| < \lambda_{so}$ and $|\Omega + U| > \lambda_{so}$, the topological index is found to be $C_{\uparrow/\downarrow}^- = -1/2$ in valley $\mathbf{K}_-$ and $C_\uparrow^+ = 1/2$ ($C_\downarrow^+ = -1/2$) in valley $\mathbf{K}_+$, and so $(C, C_s) = (-1, 1/2)$. In the same way, the topological quantum numbers in other phase regions are calculated as: CBI with (0, 0), QSHI with (0, 1), P-QHI with (−2, 0).

In Fig. 1, two phase regimes of the QSHI (0, 1) and P-QHI (−2, 0) are divided by a vertical dotted line. In only irradiation of light, the bandgap is reduced to $|V_s(\Omega)|$, where the short-hand notation is for $V_s(x) = x + s\lambda_{so}$. By substituting the Green's function Eq. (6) in spin space into Eq. (5) and then taking the matrix trace to cancel the spin degrees of freedom, the RKKY interaction can be written in the form of Eq. (7), where various coefficients are derived as $J_i = -2C\mathrm{Im}\int_{-\infty}^{E_F} N_i d\varepsilon$ $(C = 8\pi\lambda^2/\varsigma^2\hbar^4 v_F^4)$ with

$$N_\parallel = 2\left[\varepsilon^2 \cos^2\left(\frac{1}{2}\Delta\mathbf{K}\cdot\mathbf{R}\right) + \sin^2\left(\frac{1}{2}\Delta\mathbf{K}\cdot\mathbf{R}\right)\prod_{s=\pm} V_s(\Omega)\right] \prod_{s=\pm} K_0\left[\mathcal{R}_{V_s(\Omega)}\right], \tag{8}$$

$$N_z = \sum_{s=\pm}\left[\varepsilon^2\cos^2\left(\frac{1}{2}\Delta\mathbf{K}\cdot\mathbf{R}\right) + \sin^2\left(\frac{1}{2}\Delta\mathbf{K}\cdot\mathbf{R}\right)V_s^2(\Omega)\right]K_0^2\left[\mathcal{R}_{V_s(\Omega)}\right], \tag{9}$$

$$N_{DM} = -2\lambda_{so}\varepsilon\sin(\Delta\mathbf{K}\cdot\mathbf{R})\prod_{s=\pm}K_0\left[\mathcal{R}_{V_s(\Omega)}\right], \tag{10}$$

where $\Delta\mathbf{K} = \mathbf{K} - \mathbf{K}'$ is difference of momentum for any two adjacent Dirac points in BZ. We choose two valleys at $\mathbf{K}(\mathbf{K}') = \frac{2\pi}{3a}(\pm 1, \sqrt{3})$. Obviously, due to the oscillation factor $\cos(\Delta\mathbf{K}\cdot\mathbf{R})$ or $\sin(\Delta\mathbf{K}\cdot\mathbf{R})$, the RKKY interaction is closely related to spatial distance $\mathbf{R}$ between impurities. While the impurity distance fulfils $\mathbf{R} = na\hat{x}$ along the zigzag direction, the oscillating part $\sin(K_xR_x)$ repeats three values: $\frac{\sqrt{3}}{2}$, $-\frac{\sqrt{3}}{2}$, and 0, corresponding respectively to the impurity configuration satisfied $\mathrm{Mod}(R/a, 3) = 1, 2, 0$. This is indicated by A_1, A_2 and A_3 in inset of Fig. 1 while the other impurity is fixed at A_0 point. However, $\sin(\Delta\mathbf{K}\cdot\mathbf{R})$ always vanishes in the armchair direction, making the RKKY featureless, so we in the following focus on the impurities distributed along the zigzag direction and the system is half filled ($E_F = 0$).

We in Fig. 1 present the numerical results for the illumination dependence of different terms of the RKKY interaction in the long range for three types of impurity positions. For the distances satisfying $\mathrm{Mod}(R/a, 3) = 1, 2$, there emerges a prominent signature in Fig. 1(a) that the in-plane term $J_\parallel < 0$ is ferromagnetic in the QSHI phase while it changes to be antiferromagnetic in the P-QHI phase. Interestingly, the transition point is close to the critical value of phase $\Omega = \lambda_{so}$. This behavior can be understood from Eq. (8), where the second term in $N_\parallel$ plays a dominant role near the critical point and the sign of its integral is almost determined by $V_+(\Omega)V_-(\Omega) = \Omega^2 - \lambda_{so}^2$, namely, for QSHI with $|\Omega| < \lambda_{so}$ the value of $J_\parallel$ is negative while it is positive otherwise. For the impurity configuration of $\mathrm{Mod}(R/a, 3) = 0$, no such sign is observable due to $\sin(\Delta\mathbf{K}\cdot\mathbf{R/2}) = 0$. Besides, it is very interesting to find that the out-plane term J_z in Fig. 1(b) provides more accurate signature of phase transition, manifesting itself by a large dip exactly at the critical point. This dip structure occurs for all of three impurity configurations. In order to understand it, we replace the Bessel function $K_0(x)$ with $\sqrt{\pi/2x}\,e^{-x}$ in the long range[35] under consideration and taking a derivative of the N_z with respect to Ω. Finally, we obtain a result in the form of $dN_z/d\Omega \propto (\Omega - \lambda_{so})f(\Omega, \varepsilon)$, which explains the dip feature. Although J_z cannot changes sign like $J_\parallel$ when the phase transition happens, its magnitude is quantitatively different in QSHI and P-QHI phases. For the DM term J_{DM}, it keeps vanished for the Fermi energy $E_F = 0$ due to the electron-hole symmetry and the well-preserved inversion symmetry[36].

In Fig. 2(a,b), we display respectively the in-plane term $J_\parallel$ and the out-plane term J_z as a function of the illumination parameter Ω. Obviously, the transition point of the ferro-antiferromagnetism remains unchanged for different impurity distance R as long as the impurity configuration satisfying $\mathrm{Mod}(R/a, 3) = 1$ or 2. In the same way, the dip feature in J_z is also independent of the impurity distance R though the magnitude of J_z varies in different phases with increase of R. These signatures are for $E_F = 0$. We depict the case for finite Fermi level in Fig. 2(c,d), where the signatures of phase boundary can still keep robust as long as $E_F \leq \lambda_{so}$. If one further increases E_F beyond λ_{so}, the phase boundary becomes fuzzy somewhat, especially for $J_\parallel$. This can be seen easily from Eq. (8) since the first term cannot be ignored any more with increasing E_F. Figure 2(e,f) show the spatial dependence of J_z on the impurity distance R, where no difference in the order of magnitude appears in between the QSHI phase [Fig. 2(e)] and P-QHI phase [Fig. 2(d)]. At the same time, one can find the oscillation behavior, which is contributed by an additional phase factor $\cos(\Delta\mathbf{K}\cdot\mathbf{R})$. Likely, $J_\parallel$ also presents a similar scenario. The same RKKY oscillations due to the momentum difference $\Delta\mathbf{K}$ of two valleys were in detail discussed in graphene[22], which is a characteristic of bulk RKKY interaction obtained from the lattice Green's function. In ref.[16], this effect is dropped.

RKKY under electric field. We here discuss the variation of the RKKY interaction when the silicene is subject to a perpendicular electric field U. As $|U| > \lambda_{so}$, the resulting staggered potential can drive the silicene from QSHI phase to CBI phase, whose topological numbers are labeled, respectively, as (0, 1) and (0, 0) in Fig. 3. This topological phase transition is discussed in detail in refs[12,13]. For this case, we derive the RKKY interaction as $J_i = -C\mathrm{Im}\int_{-\infty}^{E_F} N_i d\varepsilon$ with

$$N_\parallel = 2\prod_{s=\pm}\zeta_s + \cos(\Delta\mathbf{K}\cdot\mathbf{R})\sum_{s=\pm}\zeta_s^2, \tag{11}$$

$$N_z = \sum_{s=\pm}\zeta_s^2 + 2\cos(\Delta\mathbf{K}\cdot\mathbf{R})\prod_{s=\pm}\zeta_s, \tag{12}$$

$$N_{DM} = \sin(\Delta\mathbf{K}\cdot\mathbf{R})\sum_s s\zeta_s^2, \tag{13}$$

where $\zeta_s = [\varepsilon - V_s(U)]K_0[\mathcal{R}_{V_s(U)}]$.

Performing the numerical calculations with above expressions, we plot the $J_\parallel$, J_z and J_{DM} terms of the exchange coupling in Fig. 3(a–c), respectively. For two impurities placed at $\mathrm{Mod}(R/a, 3) = 0$, though $J_\parallel$ and J_z present a transition from the ferromagnetic to antiferromagntic phase, the transition point is far away from the critical point $U = \lambda_{so}$. In contrast, both $J_\parallel$ and J_z for impurity configuration $\mathrm{Mod}(R/a, 3) = 1, 2$ provide a relatively accurate signature for phase boundary: a ferro-to-antiferromagntic transition for $J_\parallel$ and a dip structure for J_z. They are approximately located at the phase transition point. Very different from the case of light irradiation, J_{DM} shows a strong

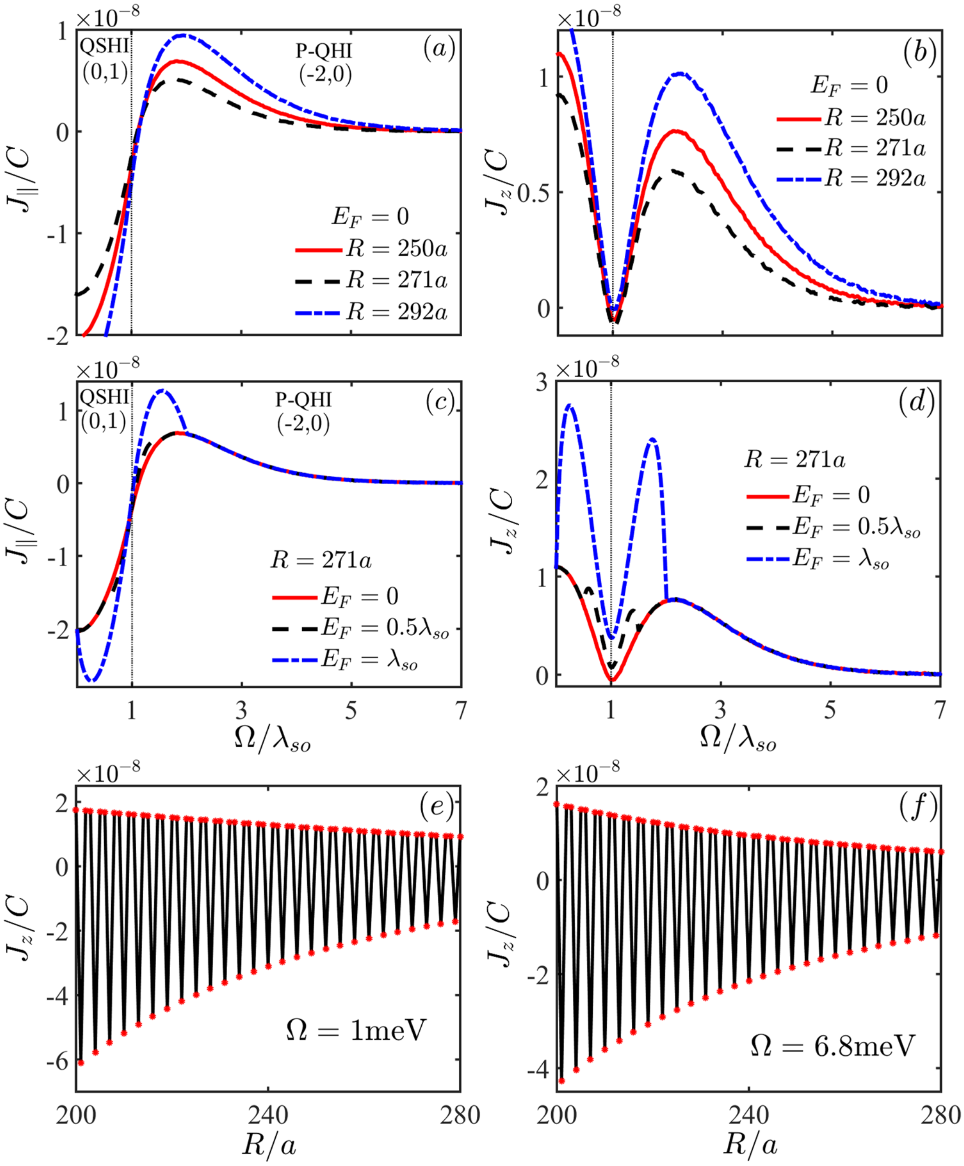

Figure 2. The dependence of $J_{\|}$ and J_z on Ω for (**a**,**b**) different impurity distances R with $E_F = 0$, (**c**,**d**) for different E_F with $R = 271a$. The spatial dependence of $J_{\|}$ and J_z for (**e**) the QSHI phase ($\Omega = 1$ meV) and (**f**) for the P-QHI phase ($\Omega = 6.8$ meV). The other parameters are the same as in Fig. 1.

dependence on the electric field as in Fig. 3(c), where Mod(R/a, 3) = 1, 2 exhibit a dip and a peak, respectively, providing an unambiguous fingerprint to ascertain the phase boundary between QSHI and CBI. In recent work[16], the authors found that the RKKY interaction of QSHI phase is about 20 times greater than that in CBI phase, and thus it is proposed to identify the topological phase transition. But, one can notice that the precondition for this signature is that the magnetic impurities must be placed at the edge of silicene where the topological edge states play a crucial role. If the impurities are deposited in bulk, this signature vanishes. On the contrary, in our study the signatures characterizing phase transition stem completely from the bulk band, regardless of the contribution of topological edge states. Thus, one can probe the topological phases simply by measurement of the bulk doping, not needing to elaborately grasp the edge-state contribution, which is experimentally accessible more easily.

RKKY under both electric and light fields. When both the electric and light fields are exerted, there emerge rich phases: QSHI, P-QHI, PS-QHI, and CBI as shown in Fig. 4(c), where the dashed lines denote the phase boundaries. Since the expressions are too tedious, we here only give the numerical results of J_z, $J_{\|}$, and J_{DM} for Mod(R/a, 3) = 1 as functions of the electric potential U and illumination parameter Ω in Fig. 4(a,b,d), respectively. Intriguingly, the phase plots in Fig. 4(a,b) present distinct changes in color in different regions, which can be used to differentiate the different phases though it is not too very strict. Importantly, J_z not only has different values for different states, but also clearly characterizes the various phase boundaries, especially for the phase transitions between PS-QHI and CBI, PS-QHI and P-QHI, and QSHI and P-QHI, where a largest dip exists. To

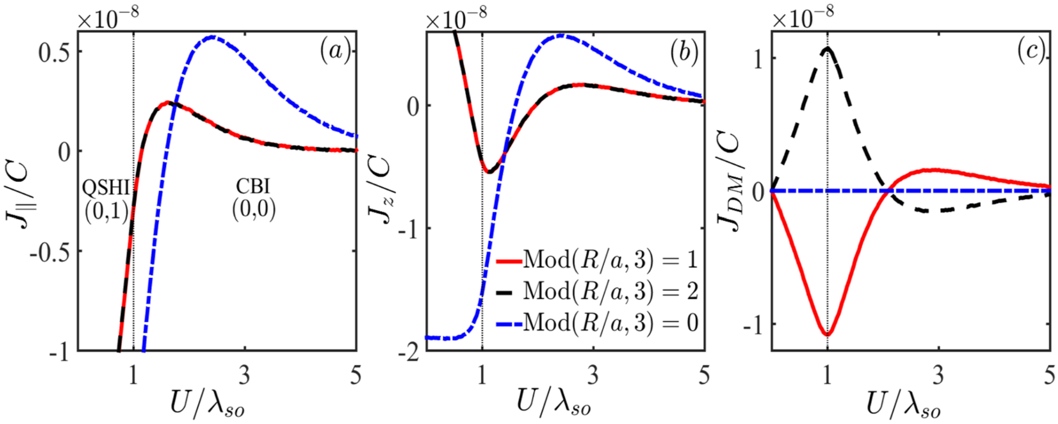

Figure 3. The dependence of (**a**) $J_\parallel$, (**b**) J_z, and (**c**) J_{DM} on the electric potential U. The others are the same as in Fig. 1.

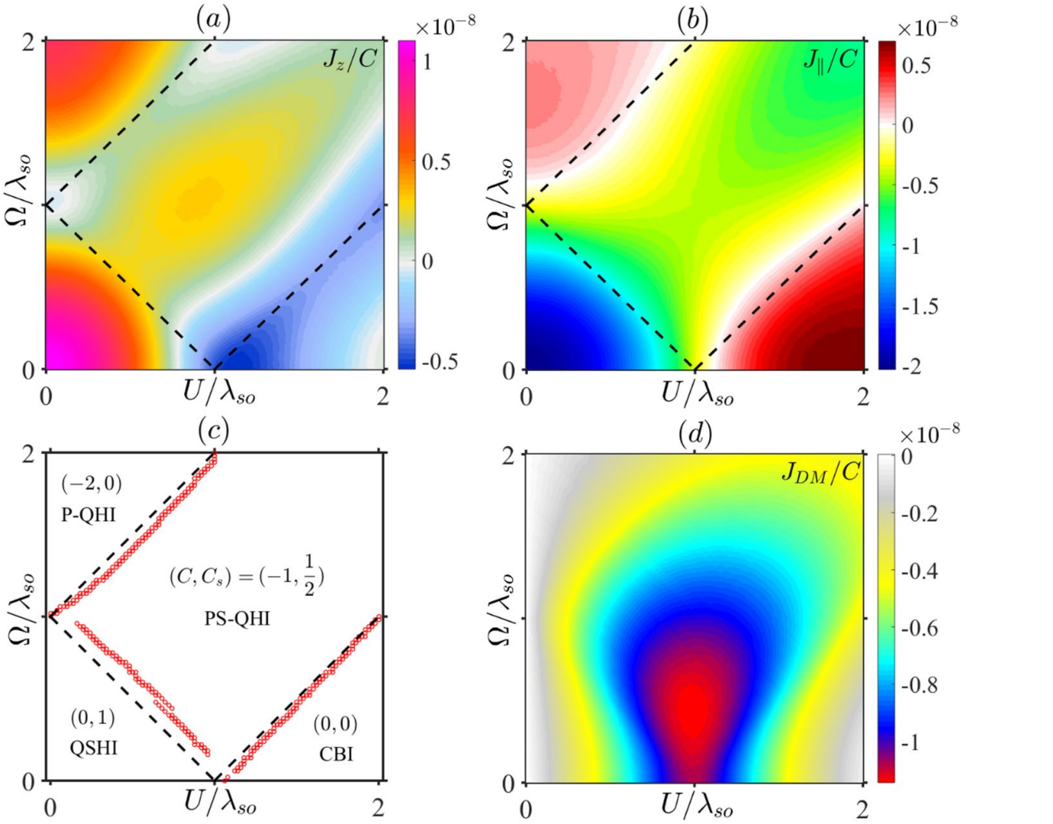

Figure 4. The phase diagrams of (**a**) J_z, (**b**) $J_\parallel$, and (**d**) J_{DM} as functions of U and Ω. (**c**) The comparison between the phase boundary (black dashed lines) and the dip position of J_z (red circles) which is selected from the local minimum value in (**a**). Different phases are labeled by different quantum numbers (C, C_s), which represent for charge- and spin-Chern numbers, respectively. The chosen parameters are $E_F = 0$ and $R = 271a$.

compare with the phase plot, we describe the characterizing signatures of the RKKY interaction in Fig. 4(c), marked with red circles by selecting the local minimal values in their boundaries. With a tolerable error, dependence of J_z on electric and light fields provides unambiguous signatures to identify the various phase transitions. By comparison, the phase boundaries of $J_\parallel$ in Fig. 4(b) become blurry but show remarkable difference in magnitude or sign for different phase regions, suitable for characterizing different phase regions. It is noted that, J_{DM} in Fig. 4(d) with a deep dip exactly at the critical point can only be applied to divide the phase transition between QSHI and CBI states, but cannot characterize the other intricate phases. As discussed above, the main reason is that J_{DM} is insensitive to irradiation. Therefore, the measurement of J_z as well as $J_\parallel$ could be a valid method to divide the different topological areas and their phase boundaries. A recent theoretical work in ref.[14] proposed that the abundant topological phases can be distinguished by measuring the Nernst conductivity. Notice that there, three types (spin, charge, and valley) of Nernst conductivity have to measure simultaneously, and then to compare them carefully to determine the phase transition boundaries. By contrast, we present an Ising RKKY diagram, from which various phases and their boundaries can be determined simultaneously only by the measurement of one type of the RKKY terms.

Conclusions

We have studied the RKKY coupling of a monolayer silicene subject to an off-resonant light and a perpendicular electric field. Due to topological phase transition, the RKKY coupling shows strong dependence on the illumination and electric potential. Based on the lattice Green's function formalism[37], we have analyzed in detail the variation of the RKKY interaction for different impurity configurations along zigzag direction. It is found that the indirect magnetic interaction has tight connection with various topological phase transitions. For the case irradiated by light, a dip structure of J_z can exactly identify the phase transition of QSHI/P-QHI while the peak or dip of J_{DM} can feature the critical point of phase transition of QSHI/CBI induced by an electric field. For more complex phase driven by both light and electric fields, it is found that J_z provides information enough to divide the different topological areas with a forgivable error in the phase boundary. Also, $J_\parallel$ exhibits remarkable difference of magnitude or sign in different phase regions though it is hard to differentiate the phase boundary. Since there are quite rare methods to detect them, especially for the phase transition between PS-QHI and P-QHI, measurement on the RKKY interaction provides us an alternative method to probe the rich topological phases in silicene or other spin-orbit systems. The underlying physics is that both the topological property and magnetic property are determined by bandgap of the band structure. Our proposal is expected to feasible with present technique of spin-polarized scanning tunneling spectroscopy[38], which can measure the magnetization curves of individual atoms.

Methods

Derivation of RKKY interaction. Starting from the effective Hamiltonian $H'_{\eta s}$ in Eq. (3), the spin- and valley- dependent retarded Green's function in **k**-space can be calculated as

$$\begin{aligned} G^{\eta s}(\mathbf{k}, \varepsilon) &= (\varepsilon + i0^{+} - H'_{\eta s})^{-1} \\ &= \frac{1}{(\varepsilon + i0^{+})^{2} - \hbar^{2}v_F^{2}k^{2} - U_{\eta s}^{2}} \begin{pmatrix} \varepsilon + U_{\eta s} & \hbar v_F k \Phi_{K_\eta} \\ \hbar v_F k \Phi_{K_\eta}^{*} & \varepsilon - U_{\eta s} \end{pmatrix}, \end{aligned} \tag{14}$$

where the matrix is in the sublattice space $\{A, B\}$. Performing a Flourier transformation from **k**-space to real space and only consider the same sublattice A,

$$\begin{aligned} G^{s}(\mathbf{R}, \varepsilon) &= \frac{1}{\varsigma}\int \sum_{\eta=\pm1} e^{i(\mathbf{k}+\mathbf{k}_\eta)\cdot\mathbf{R}} G^{\eta s}(\mathbf{k}, \varepsilon) d^{2}\mathbf{k} \\ &= \frac{2\pi}{\varsigma}\sum_{\eta=\pm1} e^{i\mathbf{K}_\eta \mathbf{R}} \int_0^\infty \frac{\varepsilon + U_{\eta s}}{(\varepsilon + i0^{+})^{2} - \hbar^{2}v_F^{2}k^{2} - U_{\eta s}^{2}} kJ_0(kR)dk \\ &= -\frac{2\pi}{\varsigma\hbar^{2}v_F^{2}}\sum_{\eta=\pm1} e^{i\mathbf{K}_\eta \mathbf{R}}(\varepsilon + U_{\eta s})K_0(\mathcal{R}_{U_{\eta s}}), \end{aligned} \tag{15}$$

which is Eq. (6) in maintext. Due to $G^{s}(\mathbf{R}, \varepsilon)$ diagonalized in spin space, the RKKY interaction of impurities in Eq. (5) is given by

$$\begin{aligned} H_{RKKY} &= \frac{-\lambda^{2}}{\pi}\mathrm{Im}\int_{-\infty}^{E_F} \mathrm{Tr}[(\mathbf{S}_1\cdot\sigma)G(\mathbf{R}, \varepsilon)(\mathbf{S}_2\cdot\sigma)G(-\mathbf{R}, \varepsilon)]d\varepsilon \\ &= \frac{-\lambda^{2}}{\pi}\mathrm{Im}\int_{-\infty}^{E_F} \sum_{i,j=x,y,z} S_{1i}S_{2j}\mathrm{Tr}\big[\sigma_i G(\mathbf{R}, \varepsilon)\sigma_j G(-\mathbf{R}, \varepsilon)\big]d\varepsilon. \end{aligned} \tag{16}$$

Inserting the Green's function $G(\mathbf{R},\varepsilon)$ in Eq. (15) into the above equation and calculating the trace of the matrix product $\sigma_i G(\mathbf{R}, \varepsilon)\sigma_j G(-\mathbf{R}, \varepsilon)$ over the spin, the RKKY interaction can be divided into three parts

$$H_{RKKY} = J_\parallel \sum_{i=x,y} S_{1i}S_{2i} + J_z S_{1z}S_{2z} + J_{DM}(\mathbf{S}_1 \times \mathbf{S}_2)_z, \tag{17}$$

where

$$J_\parallel = \frac{-\lambda^{2}}{\pi}\mathrm{Im}\int_{-\infty}^{E_F} [G_{+}(\mathbf{R}, \varepsilon)G_{-}(-\mathbf{R}, \varepsilon) + G_{-}(\mathbf{R}, \varepsilon)G_{+}(-\mathbf{R}, \varepsilon)]d\varepsilon, \tag{18}$$

$$J_z = \frac{-\lambda^{2}}{\pi}\mathrm{Im}\int_{-\infty}^{E_F} [G_{+}(\mathbf{R}, \varepsilon)G_{+}(-\mathbf{R}, \varepsilon) + G_{-}(\mathbf{R}, \varepsilon)G_{-}(-\mathbf{R}, \varepsilon)]d\varepsilon, \tag{19}$$

$$J_{DM} = \frac{-\lambda^2}{\pi}\mathrm{Re}\int_{-\infty}^{E_F}[G_-(\mathbf{R},\varepsilon)G_+(-\mathbf{R},\varepsilon) - G_+(\mathbf{R},\varepsilon)G_-(-\mathbf{R},\varepsilon)]d\varepsilon. \tag{20}$$

For the radiation with light field, $U_{\eta s} = \eta V_s(\Omega) = \eta(\Omega + s\lambda_{so})$. With the help of Eqs (15) and (18), one can simplify the RKKY component $J_\parallel$ as

$$\begin{aligned} J_\parallel &= -\frac{4\pi\lambda^2}{\varsigma^2\hbar^4v_F^4}\mathrm{Im}\int_{-\infty}^{E_F}\left[\sum_{\eta,\eta'=\pm1}e^{i(\mathbf{K}_\eta-\mathbf{K}_{\eta'})\mathbf{R}}(\varepsilon+\eta V_+)(\varepsilon+\eta' V_-)K_0\left(\mathcal{R}_{V_+}\right)K_0(\mathcal{R}_{V_-})\right]d\varepsilon \\ &\quad -\frac{4\pi\lambda^2}{\varsigma^2\hbar^4v_F^4}\mathrm{Im}\int_{-\infty}^{E_F}\left[\sum_{\eta,\eta'=\pm1}e^{i(\mathbf{K}_\eta-\mathbf{K}_{\eta'})\mathbf{R}}(\varepsilon+\eta V_-)(\varepsilon+\eta' V_+)K_0(\mathcal{R}_{V_-})K_0\left(\mathcal{R}_{V_+}\right)\right]d\varepsilon \\ &= -\frac{32\pi\lambda^2}{\varsigma^2\hbar^4v_F^4}\mathrm{Im}\int_{-\infty}^{E_F}\left[\varepsilon^2\cos^2\left(\frac{1}{2}\Delta\mathbf{K}\cdot\mathbf{R}\right)+\sin^2\left(\frac{1}{2}\Delta\mathbf{K}\cdot\mathbf{R}\right)\prod_{s=\pm}V_s(\Omega)\right] \\ &\quad \prod_{s=\pm}K_0\left[\mathcal{R}_{V_s(\Omega)}\right]d\varepsilon. \end{aligned}$$

We denote $J_i = -2C\mathrm{Im}\int_{-\infty}^{E_F}N_i d\varepsilon\,(C = 8\pi\lambda^2/\varsigma^2\hbar^4v_F^4)$, and so

$$N_\parallel = 2\left[\varepsilon^2\cos^2\left(\frac{1}{2}\Delta\mathbf{K}\cdot\mathbf{R}\right)+\sin^2\left(\frac{1}{2}\Delta\mathbf{K}\cdot\mathbf{R}\right)\prod_{s=\pm}V_s(\Omega)\right]\prod_{s=\pm}K_0\left[\mathcal{R}_{V_s(\Omega)}\right]. \tag{21}$$

Similarly, the other RKKY components $N_\parallel$ and N_{DM} can be obtained to be Eqs (9) and (10).

In applied electric field where $U_{\eta s} = \eta V_s(U) = U + \eta s\lambda_{so}$, one can perform the same procedure, and the RKKY interaction in Eqs (11–13) are also obtained.

References

1. Price, H. M., Zilberberg, O., Ozawa, T., Carusotto, I. & Goldman, N. Measurement of Chern numbers through center-of-mass responses. *Phys. Rev. B* **93**, 245113 (2016).
2. Hasan, M. Z. & Kane, C. L. Colloquium: Topological insulators. *Rev. Mod. Phys.* **82**, 3045 (2010).
3. Qi, X.-L. & Zhang, S.-C. Topological insulators and superconductors. *Rev. Mod. Phys.* **83**, 1057 (2011).
4. Sothmann, B. & Hankiewicz, E. M. Fingerprint of topological Andreev bound states in phase-dependent heat transport. *Phys. Rev. B* **94**, 081407(R) (2016).
5. Swingle, B. Experimental signatures of three-dimensional fractional topological insulators. *Phys. Rev. B* **86**, 245111 (2012).
6. Mikitik, G. P. & Sharlai, Y. V. Magnetic susceptibility of topological nodal semimetals. *Phys. Rev. B* **94**, 195123 (2016).
7. Kernreiter, T., Governale, M., Zülicke, U. & Hankiewicz, E. M. Anomalous Spin Response and Virtual-Carrier-Mediated Magnetism in a Topological Insulator. *Phys. Rev. X* **6**, 021010 (2016).
8. Vogt, P. *et al.* Silicene: Compelling Experimental Evidence for Graphenelike Two-Dimensional Silicon. *Phys. Rev. Lett.* **108**, 155501 (2012).
9. Fleurence, A. *et al.* Experimental Evidence for Epitaxial Silicene on Diboride Thin Films. *Phys. Rev. Lett.* **108**, 245501 (2012).
10. Chen, L. *et al.* Evidence for Dirac Fermions in a Honeycomb Lattice Based on Silicon. *Phys. Rev. Lett.* **109**, 056804 (2012).
11. Liu, C.-C., Jiang, H. & Yao, Y. Low-energy effective Hamiltonian involving spin-orbit coupling in silicene and two-dimensional germanium and tin. *Phys. Rev. B* **84**, 195430 (2011).
12. Drummond, N. D., Zólyomi, V. & Fal'ko, V. I. Electrically tunable band gap in silicene. *Phys. Rev. B* **85**, 075423 (2012).
13. Ezawa, M. Photoinduced Topological Phase Transition and a Single Dirac-Cone State in Silicene. *Phys. Rev. Lett.* **110**, 026603 (2013).
14. Xu, Y., Zhou, X. & Jin, G. Detecting topological phases in silicene by anomalous Nernst effect. *Appl. Phys. Lett.* **108**, 203104 (2016).
15. Imamura, H., Bruno, P. & Utsumi, Y. Twisted exchange interaction between localized spins embedded in a one- or two-dimensional electron gas with Rashba spin-orbit coupling. *Phys. Rev. B* **69**, 121303(R) (2004).
16. Zare, M., Parhizgar, F. & Asgari, R. Topological phase and edge states dependence of the RKKY interaction in zigzag silicene nanoribbon. *Phys. Rev. B* **94**, 045443 (2016).
17. Min, H. *et al.* Intrinsic and Rashba spin-orbit interactions in graphene sheets. *Phys. Rev. B* **74**, 165310 (2006).
18. Yao, Y., Ye, F., Qi, X.-L., Zhang, S.-C. & Fang, Z. Spin-orbit gap of graphene: First-principles calculations. *Phys. Rev. B* **75**, 041401(R) (2007).
19. Takeda, K. & Shiraishi, K. Theoretical possibility of stage corrugation in Si and Ge analogs of graphite. *Phys. Rev. B* **50**, 14916 (1994).
20. Durgun, E., Tongay, S. & Ciraci, S. Silicon and III-V compound nanotubes: Structural and electronic properties. *Phys. Rev. B* **72**, 075420 (2005).
21. Cahangirov, S., Topsakal, M., Aktürk, E., Şahin, H. & Ciraci, S. Two- and One-Dimensional Honeycomb Structures of Silicon and Germanium. *Phys. Rev. Lett.* **102**, 236804 (2009).
22. Sherafati, M. & Satpathy, S. RKKY interaction in graphene from the lattice Green's function. *Phys. Rev. B* **83**, 165425 (2011).
23. Oka, T. & Aoki, H. Photovoltaic Hall effect in graphene. *Phys. Rev. B* **79**, 081406(R) (2009).
24. Inoue, J.-I. & Tanaka, A. Photoinduced Transition between Conventional and Topological Insulators in Two-Dimensional Electronic Systems. *Phys. Rev. Lett.* **105**, 017401 (2010).
25. Kitagawa, T., Oka, T., Brataas, A., Fu, L. & Demler, E. Transport properties of nonequilibrium systems under the application of light: Photoinduced quantum Hall insulators without Landau levels. *Phys. Rev. B* **84**, 235108 (2011).
26. Lindner, N. H., Refael, G. & Galitski, V. Floquet Topological Insulator in Semiconductor Quantum Wells. *Nat. Phys.* **7**, 490 (2011).
27. Dóra, B., Cayssol, J., Simon, F. & Moessner, R. Optically Engineering the Topological Properties of a Spin Hall Insulator. *Phys. Rev. Lett.* **108**, 056602 (2012).
28. López, A., Scholz, A., Santos, B. & Schliemann, J. Photoinduced pseudospin effects in silicene beyond the off-resonant condition. *Phys. Rev. B* **91**, 125105 (2015).
29. Li, H., Sheng, L. & Xing, D. Y. Connection of Edge States to Bulk Topological Invariance in a Quantum Spin Hall State. *Phys. Rev. Lett.* **108**, 196806 (2012).
30. Ruderman, M. A. & Kittel, C. Indirect Exchange Coupling of Nuclear Magnetic Moments by Conduction Electrons. *Phys. Rev.* **96**, 99 (1954).

31. Kasuya, T. Electrical Resistance of Ferromagnetic Metals. *Prog. Theor. Phys.* **16**, 58 (1956).
32. Yosida, K. Magnetic properties of Cu-Mn alloys. *Phys. Rev.* **106**, 893 (1957).
33. Chesi, S. & Loss, D. RKKY interaction in a disordered two-dimensional electron gas with Rashba and Dresselhaus spin-orbit couplings. *Phys. Rev. B* **82**, 165303 (2010).
34. Tuan, D. V. *et al.* Spin Hall Effect and Origins of Nonlocal Resistance in Adatom-Decorated Graphene. *Phys. Rev. Lett.* **117**, 176602 (2016).
35. Saremi, S. RKKY in half-filled bipartite lattices: Graphene as an example. *Phys. Rev. B* **76**, 184430 (2007).
36. Chang, H.-R., Zhou, J., Wang, S.-X., Shan, W.-Y. & Xiao, D. RKKY interaction of magnetic impurities in Dirac and Weyl semimetals. *Phys. Rev. B* **92**, 241103(R) (2015).
37. Horiguchi, T. Lattice Green's Functions for the Triangular and Honeycomb Lattices. *J. Math. Phys.* **13**, 1411 (1972).
38. Zhou, L. *et al.* Strength and directionality of surface Ruderman-Kittel-Kasuya-Yosida interaction mapped on the atomic scale. *Nat. Phys.* **6**, 187 (2010).

Acknowledgements

This project was supported by GDUPS (2017), by NSF of China (Grant Nos 11474106, 61771206, and 11274124), by Guangdong key NSF of China (Grant No. 2017B030311003), and by the Innovation Project of Graduate School of South China Normal University.

Author Contributions

R.Q.W. conceived the idea. H.J.D. and C.W. performed the calculation. H.J.D. and C.W. provided the figures. R.Q.W. and H.J.D. wrote the manuscript. S.H.Z., M.Y., and D.R.P. joined in the data analysis and contributed to the discussion. All authors reviewed the manuscript.

Additional Information

Competing Interests: The authors declare no competing interests.

Publisher's note: Springer Nature remains neutral with regard to jurisdictional claims in published maps and institutional affiliations.